Journal of The Electrochemical Society, 2022 **169** 043509
1945-7111/2022/169(4)/043509/10/$40.00 © 2022 The Electrochemical Society ("ECS"). Published on behalf of ECS by IOP Publishing Limited

Electrochemical Polishing of Tungsten: An Investigation of Critical Spatial Frequency and Ultimate Roughness

Ji Jianwei,[1] Khan Muhammad Ajmal,[2] Zhan Zejin,[2] Yi Rong,[2] and Deng Hui[2,z]

[1]*Academy for Advanced Interdisciplinary Studies, Southern University of Science and Technology, No. 1088, Xueyuan Road, Shenzhen, Guangdong 518055, People's Republic of China*
[2]*Department of Mechanical and Energy Engineering, Southern University of Science and Technology, No. 1088, Xueyuan Road, Shenzhen, Guangdong 518055, People's Republic of China*

Electrochemical polishing (ECP) offers incomparable advantages and great potential in metal polishing by surface errors correction. This paper systematically investigates the ultimate roughness and surface errors correction ability of ECP over different spatial frequency ranges. This paper further explores the law of ECP influencing errors at different frequency ranges, proposes and clarifies the concept of critical spatial frequency, and studies the law of polishing parameters affecting critical spatial frequency by using spatial frequency spectrum analysis. The surface roughness evolution and ultimate roughness of ECP were investigated using the surface error filtering method based on the critical spatial frequency. The ultimate roughness of ECP was determined by two different strategies, (i) stepwise polishing and (ii) one-step polishing. In addition, the stepwise polishing was also investigated for any possible inconsistency with one-step polishing on the final surface roughness. As ECP progressed, the optimization speed of surface roughness gradually decreased, and the surface roughness eventually reached a stable limiting value. Further analysis revealed that crystal corrosion is mainly responsible for inhibiting surface roughness optimization.
 [DOI: 10.1149/1945-7111/ac63fa]

Manuscript submitted January 24, 2022; revised manuscript received March 18, 2022. Published April 14, 2022.

Tungsten is a chemically stable rare refractory metal with high values of melting point (3410 °C), hardness, and wear resistance.[1,2] In addition to being widely used as a cutting tool in the form of alloy, tungsten is a common mold material[3] because of its high hardness, and serves in nuclear fusion reactors[4] under extremely harsh conditions, such as high temperature, high pressure, and high corrosion. These applications demand top-notch surface finishing, but the extreme hardness, wear resistance, and high chemical stability are challenging efficient and ultra-precision polishing of tungsten.

The conventional polishing methods cannot realize high-efficiency, super smooth, scratchless, and damage-free polishing of intricate tungsten components. For example, mechanical polishing[5] induces scratches and subsurface damage to the surface and cause wear of the grinding wheel. Chemical mechanical polishing (CMP)[6] offers low material removal efficiency and is inappropriate for polishing complex geometries. Diamond turning[7] creates residual turning marks on the processed surface, whereas turning ultrahard material shortens the tool life due to severe wear. Wire electrical discharge machining (WEDM)[8] has high removal efficiency, but high operating temperatures generate heat-affected zones (HAZ) on the machined surface.

ECP is an anodic dissolution-based metal material-removing technology.[9,10] This technique is advantageous because of its high material removal efficiency, allowance for complex geometries, and no subsurface damage, unlike previously mentioned metal polishing methods. Therefore, ECP has great potential and has been widely used for processing tungsten and other superhard alloys reported in the literature.[11–13] Deng et al.[14] classified electrochemical machining into current-driven ECP and potential-driven ECP based on the difference in electrolyte conductivity and analyzed their characteristics. According to the results, the current-driven ECP offered high material removal rate, suitable for removing subsurface damages and grinding marks, while the potential-driven ECP realized ultrasmooth surface by improving the surface roughness. Wang et al.[15] analyzed the influence of voltage, and based on the results, the ECP of tungsten was divided into three stages: etching, brightening, and pitting. The possible material removal mechanisms during different stages were proposed and verified by experiments. Han et al.[16] compared the similarities and differences between the acidic and alkaline electrolytes and investigated the interelectrode gap influence on the polishing results. The preceding discussions have shown that optimizing polishing parameters, such as applied voltage, current, and electrolyte concentration, have been the key research focus. Although these parameters have primary importance in ECP, determining the critical spatial frequency and ultimate roughness of ECP seek considerable attention.

A surface error is well known to be composed of a series of different spatial frequency errors. Typically, a surface error can be decomposed into surface roughness, waviness, and shape, corresponding to high, middle, and low spatial frequency errors, respectively. A high-quality surface roughness enhancement can make a surface glossy, eliminate surface defects and improve the corrosion resistance of parts. The surface waviness error can seriously aggravate the distinctness of image (DOI) from a surface, sealing quality of a sealing ring, sliding vibration of the ball bearing, etc. The specific division method of surface roughness and waviness vary according to different applications. Processing methods significantly affect the errors related to different spatial frequency bands on the surface. For example, diamond fly-cutting[17] and computer-controlled optical surfacing (CCOS) technology[18] can optimize the low-frequency error while worsening the waviness error. Continuous polishing technology[19] can optimize the waviness error and surface roughness, but the ability to control the shape error is limited. Typically, the ECP, which is good at optimizing the surface roughness, cannot correct the waviness and surface shape error. However, the frequency range that ECP can correct is rarely mentioned and studied.

In addition to the correction ability of different spatial frequency errors, the ultimate roughness of ECP technology is also a topic worthy of further exploration. Although the polishing ability of ECP has been fully proved, the surface quality is higher, the better in practical applications. For example, in molding technology, demolding becomes easier for a better quality surface. Similarly, super lubrication is another fine example of improved surface quality. Since higher surface quality produces less friction and nullifies the energy loss when surface roughness approaching the ideal zero. In addition, the requirements for surface processing accuracy and quality are hiking with the everyday development of science and technology, which poses a challenge to the ultimate roughness of ECP. Therefore, the ultimate roughness level that ECP can achieve and the reasons that hinder further optimization of surface roughness should be explored. These explorations might establish foundations for the further improvement of the accuracy of ECP technology.

[z]E-mail: dengh@sustech.edu.cn

Based on the above analysis, this paper focuses on two fundamental and exclusive problems of ECP; (i) critical spatial frequency and (ii) ultimate roughness. This paper experimentally studies and ascertains the spatial frequency error that ECP can correct. In addition, the evolution of surface roughness and ultimate roughness during ECP are explored. Further analysis reveals that crystal corrosion is responsible for the ultimate roughness.

Experimental Methods

Workpiece preparation and the experiment setup.—Tungsten samples (Xin Ji Metal Materials Co., Ltd.) used in experiments are more than 99.99% pure and taken from the same batch to ensure the uniformity of the material composition. The size of the workpiece is $13 \times 13 \times 3$ mm^3. Firstly, the as-received substrates were ground for 10 min with #180 grit sandpaper to remove turning marks, oxide layer, and possible oil stains. The samples were further grounded for 30 s by a new #180 grit sandpaper with a linear reciprocating motion to obtain the grinding traces along a specific direction. Finally, the samples were ground for 10 s with #600 grit sandpaper in the same order. After grinding, the samples were ultrasonically cleaned with deionized water for 10 min, and then with alcohol for the same duration. The roughness of the surface obtained by this process is about 200 nm, which is nearly uniform throughout the workpiece surface. All the samples in this paper, unless otherwise specified, were prepared following the same surface treatment to obtain similar initial roughness and micro-morphology.

Figure 1a shows the schematic diagram of the experimental equipment. The workpiece was connected to the anode of the DC power supply. During the polishing process, only the front face (13×13 mm^2) of the workpiece was exposed to the electrolyte, while an insulating clamp covered the rest of the substrate. The cathode was a platinum sheet with an area of 20×20 mm^2. The Z-movement of the positioning platform controlled the immersion depth of the workpiece, while the designed fixture was adjustable for the desired interelectrode gap. The polishing voltage was provided by the Keysight E3649A dual-channel DC power supply, and the real-time polishing current can be obtained via Kickstart software. The analytical grade NaOH electrolyte used in this study was provided by Merck, Germany. The samples after ECP were ultrasonically cleaned with deionized water and alcohol each for 10 min. Figure 1b shows the most widely accepted viscous layer theory.[20,21] The dissolved metallic products accumulate on the anode surface and form a highly resistive viscous layer during ECP. The viscous layer thickness determines its electrical resistance and the dissolution rate of the metal.

Surface morphology and power spectral density (PSD).—The surface roughness before and after polishing was measured by white light interferometer (WLI, Taylor Hobson M112–4449–02 CCI HD) with a 10X objective lens and 4 M measurement setting. The image was obtained from 1.66×1.66 mm^2 area, with a total of 2048×2048 pixels, so each pixel represented an area of 0.81×0.81 μm^2. The definition of average surface roughness *Sa* (ISO25178) is as follows:

$$Sa = \frac{1}{A}\int_A |z(x, y)|\, dxdy \qquad [1]$$

where A means the measurement area, $|z(x, y)|$ is the distance from any point on the surface to the reference plane.

The *Sa* roughness largely depends on the selected measurement position. To eliminate the error caused by the random positions measurement and accurately evaluate the polishing ability of ECP, the analysis method of repeated positioning was used. The details about the repeated positioning method and the analysis of positioning accuracy can be found in Ref. 22. A scanning electron microscope (SEM, Hitachi TM4000Plus) was used to investigate the surface morphology. The material removed after polishing was determined by a precision electronic balance (Mettler Toledo, ME203). Combined with the density of tungsten and the shape of the workpiece, the material removal thickness can be easily calculated.

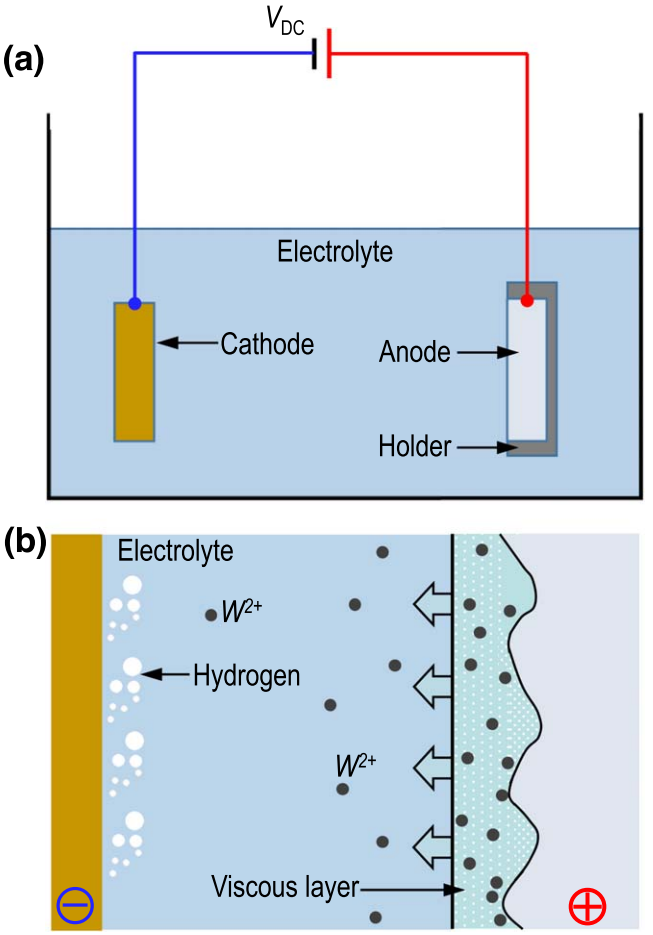

Figure 1. Schematic of (a) the ECP experimental setup and (b) the development of viscous layer during ECP.

This paper uses the power spectral density (PSD) function method to analyze and evaluate the ability of ECP to correct different spatial frequency errors. The PSD method is also a surface quality evaluation method similar to the surface roughness characterization method. However, the traditional surface roughness *Sa* characterization method can only provide information related to the surface micro-morphology, and surface frequency information remains missing. Therefore, it is insufficient to analyze the surface quality by using the traditional characterization parameters only. PSD method converts the spatial description of the error into the frequency distribution by using the Fourier transform of the discrete data obtained from the surface measurement. The PSD function has been a generic method for surface characterization and analysis, widely used in industrial production, such as functional evaluation of optical systems.[23–25] The one-dimensional PSD function is defined as the square of the Fourier spectral amplitude of each frequency component of the wavefront. Its mathematical form is as follows:

$$PSD(v_i) = \frac{(A(v_i))^2}{\Delta v} \qquad [2]$$

where v_i is spatial frequency, Δv is the increment between frequencies, $A(v_i)$ is the Fourier amplitude at the frequency v_i.

Ultimate roughness.—It is widely accepted that ECP can efficiently realize the ultra-precision polishing of metal and alloys,

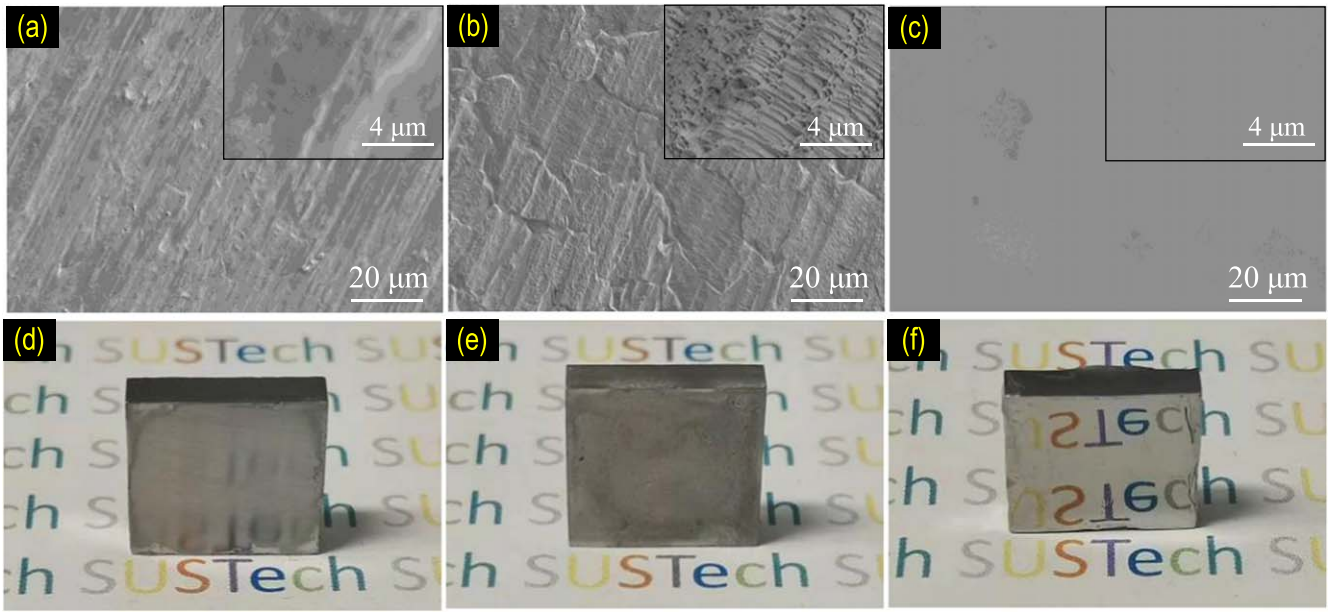

Figure 2. SEM morphologies and images of the tungsten surfaces. (a), (d) The original surface processed by #600 grit sandpaper; (b), (e) the surface processed by ECP at 2 V for 600 s; (c), (f) surface processed by ECP at 15 V for 600 s. Insets in (a)–(c): SEM morphologies at high magnification (10 k).

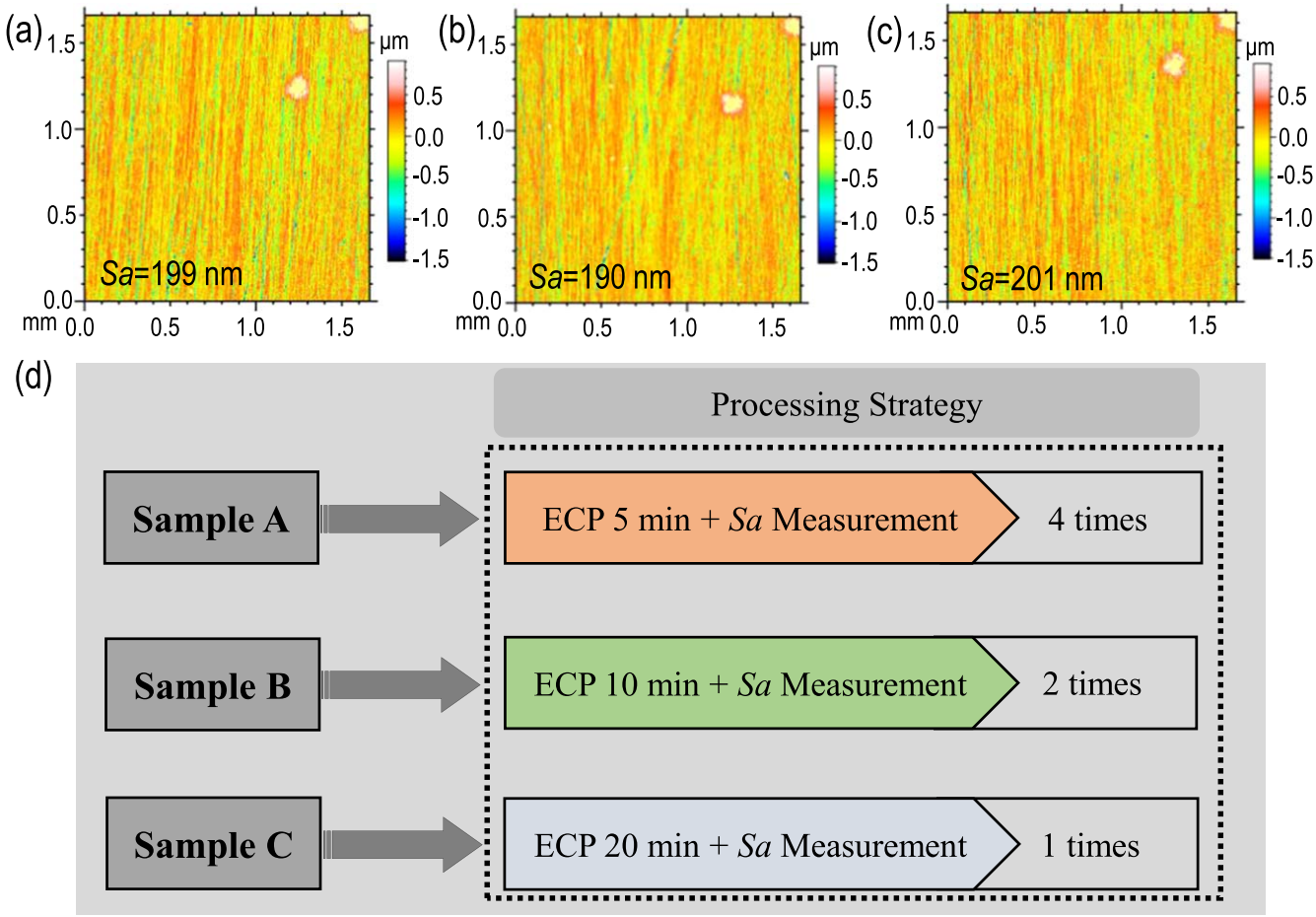

Figure 3. WLI morphologies and the *Sa* roughness of (a) Sample A, (b) Sample B, (c) Sample C, before ECP, and (d) the stepwise and one-step polishing strategies designed for a total of 20 min duration.

and the *Sa* roughness can be gradually optimized by extending the polishing duration.[26–28] However, as mentioned earlier, determining the ultimate roughness and exploring the factors hindering further surface optimization by ECP have rarely been studied. Therefore, this paper presents exclusive experiments on determining the ultimate roughness and the factors impeding further surface optimization. It should be noted that the ECP of tungsten shown in Fig. 2 presents different surfaces processed under different voltage

Table I. Details of the experimental parameters and obtained results.

	Experiment set 1			Experiment set 2		
Parameter/Sample	A	B	C	A	B	C
Voltage (V)	10	20	30	15	15	15
NaOH concentrations (wt%)	1%	1%	1%	0.5%	1%	1.5%
Polishing time (min)	34	13	9	76	23	16
Mass difference (g)	0.055	0.056	0.059	0.063	0.066	0.063

conditions. When the voltage is low (<5 V), the insufficient current density cannot generate a viscous layer, so the ECP process remains in the etching state. Surface polishing is achieved when the voltage or current density is large enough to form a viscous layer on the workpiece surface. This point has been fully discussed in Wang's paper[15] and ECP of tungsten with different applied potentials was divided into 3 stages: etching stage, brightening stage and pitting stage. This paper investigates the ultimate roughness when ECP is operated in the brightening stage or with polishable parameters.

The ECP ultimate roughness experiments were conducted over a surface with initial *Sa* roughness of ~200 nm. The substrate was polished using a stepwise polishing strategy until the *Sa* roughness did not change further. The repeated positioning method was used to ensure the same position measurement before and after ECP. The substrate was polished for 200 min in total. Initially, the *Sa* roughness was measured every 10 min; however, the roughness optimization rate was reduced with decreasing *Sa* roughness, so the polishing interval was increased to 15 min

Critical spatial frequency.—It is generally known that the *Sa* roughness results exclusively depend on the evaluation methods. Different measuring instruments or filtering frequencies result in distinct spatial frequency bands; ultimately, the obtained results become incomparable. Therefore, selecting measuring instruments and filtering frequency is very important when evaluating the polishing ability of ECP technology, which can seriously affect the experimental results. As discussed in the part of Introduction, ECP can only correct the roughness error, but optimizing errors at the low and middle spatial frequencies is not possible with ECP. This means ECP has obvious selectivity of spatial frequency error correction. However, what is the spatial frequency error range that ECP can correct? How is the correction capability of ECP? How do the processing parameters affect the correction range? These questions are very meaningful but rarely addressed. The lowest frequency that ECP can correct can be defined as critical spatial frequency (f_c), and the corresponding spatial period is called the critical period. So ECP can only correct the frequency band error higher than the critical spatial frequency, while it is difficult to correct the frequency band errors lower than the critical spatial frequency. Therefore, the critical spatial frequency was taken as the filtering frequency to reduce interference from low and middle-frequency errors for accurately determining the ultimate roughness and polishing ability of ECP.

A series of experiments were designed to explore the critical spatial frequency of ECP and the effects of polishing voltage and electrolyte concentration on the critical spatial frequency. The

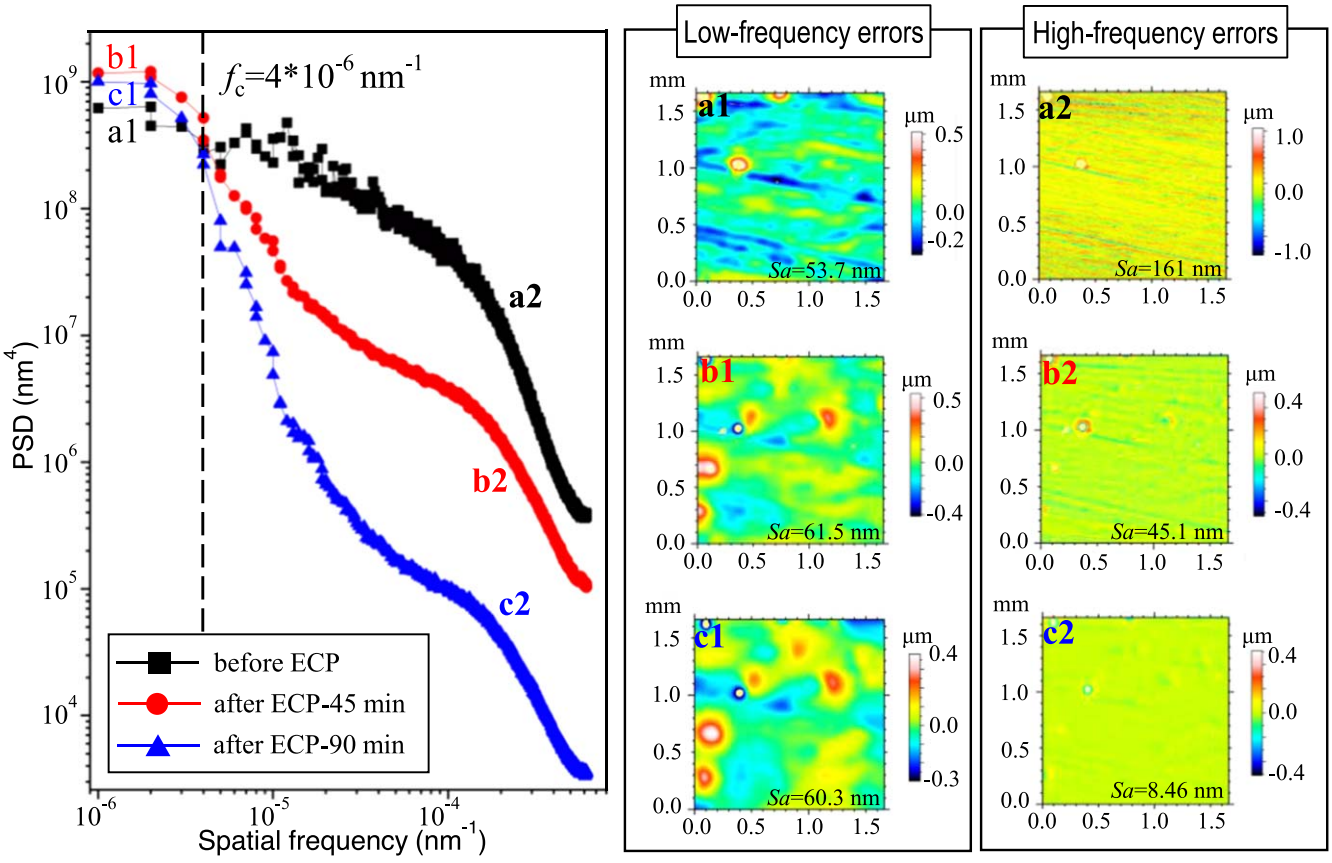

Figure 4. PSD curves, low-frequency errors and high frequency errors before and after ECP for 45 min and 90 min.

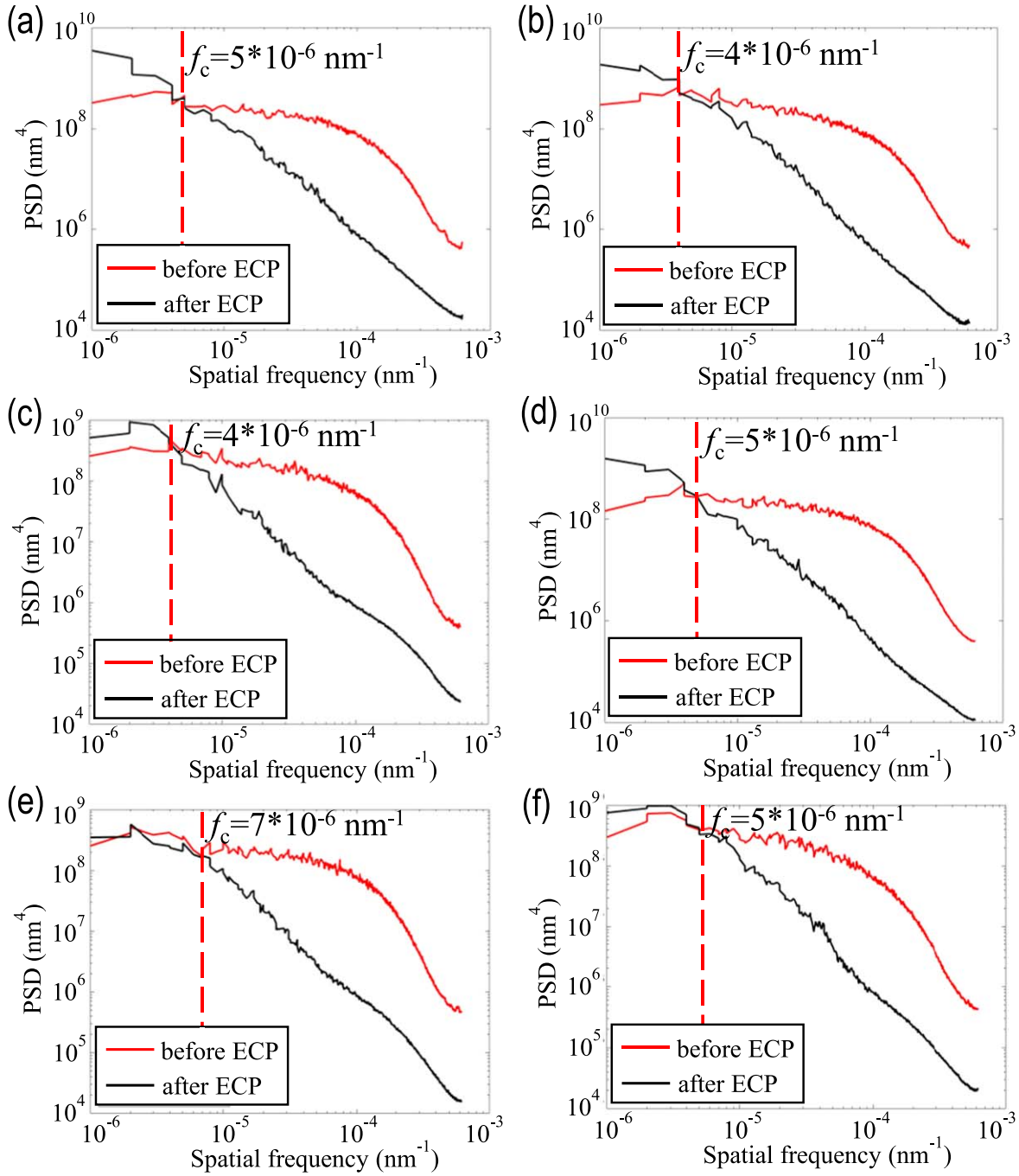

Figure 5. The PSD curves before and after ECP with different polishing parameters: (a) U = 10 V, c = 1%; (b) U = 20 V, c = 1%; (c) U = 30 V, c = 1%; (d) U = 15 V, c = 0.5%; (e) U = 15 V, c = 1%; and (f) U = 15 V, c = 1.5%.

detailed experimental parameters are given in Table I. In experiment set 1, the effect of different voltages (10 V, 15 V, 20 V) on critical spatial frequency was investigated under the same electrolyte concentration (1%). In experiment set 2, the effect of different electrolyte concentrations (0.5%, 1%, 1.5%) on critical spatial frequency was investigated under the same polishing voltage (15 V). The initial surfaces of all workpieces used in these experiments were similar and obtained strictly following the process described in the part of Workpiece Preparation. In these experiments, the same material removal thickness was achieved under different polishing parameters by fine-tuning the polishing duration. The repeated positioning method ensured the same position measurement before and after polishing.

Stepwise polishing and one-step polishing.—To derive the law of *Sa* roughness evolution and explore the ultimate roughness as a function of time, the substrate polishing and characterization are performed in alternating order. For example, the substrate is polished for a certain time, removed from the electrolyte, ultrasonically cleaned, characterized for roughness, and polished again under the same experimental conditions. This process continues unless the surface roughness becomes almost constant. Such a polishing strategy can be defined as "stepwise polishing." In contrast, if a workpiece is continuously polished for a planned duration, it is defined as "one-step polishing." The influence of stepwise polishing on the final surface quality after ECP is ambiguous. Therefore, it is necessary to investigate any possible inconsistencies between the

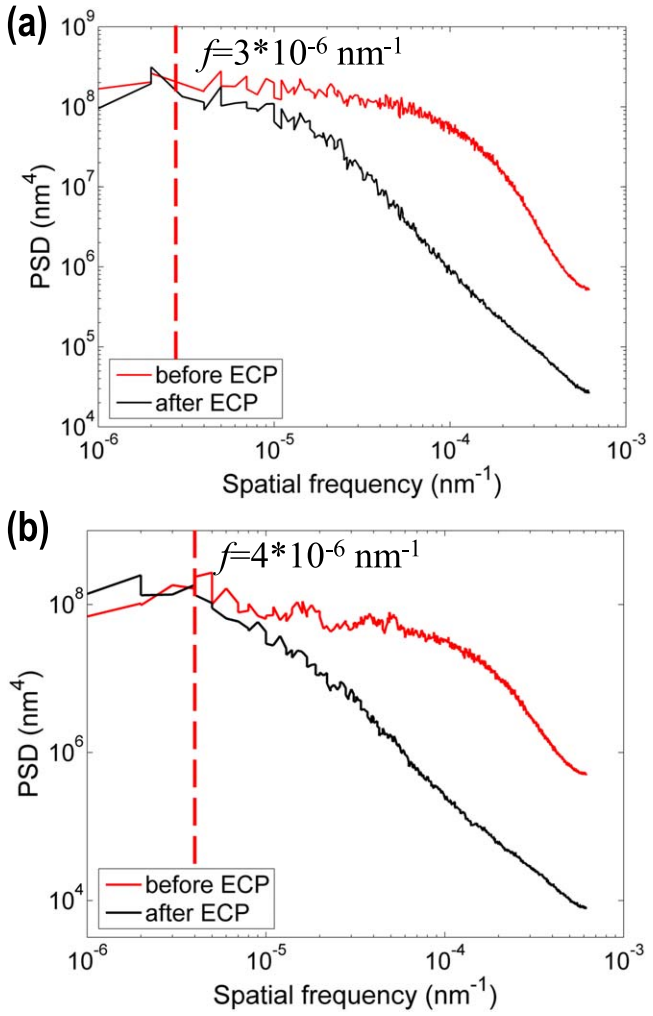

Figure 6. The PSD curves before and after ECP with different initial surface roughness: (a) *Sa* = 150 nm; (b) *Sa* = 150 nm.

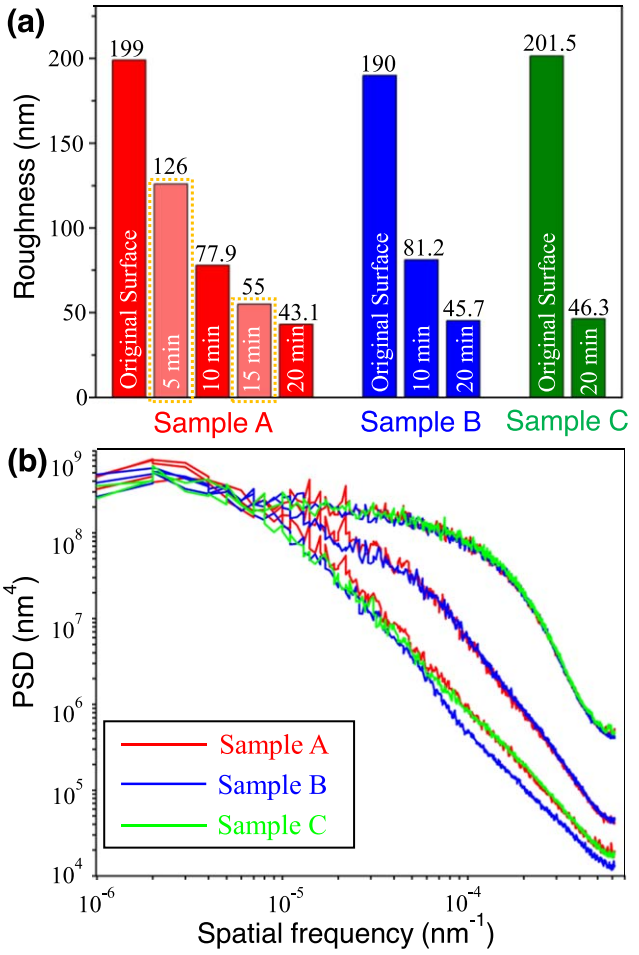

Figure 7. Comparison of stepwise polishing and one-step polishing: (a) *Sa* roughness, and (b) PSD curves. The PSD curves of the two groups of data with black dotted lines are not presented.

polishing results of stepwise and one-step polishing before the ECP ultimate roughness exploration. It is also necessary to ensure the rationality of stepwise polishing in the ECP ultimate roughness exploration experiment.

The processing strategy for the comparative study of stepwise and one-step polishing is shown in Fig. 3. In these experiments, three samples A, B, and C, with similar initial *Sa* roughness 199 nm, 190 nm, and 201 nm, respectively, are used. Their initial morphologies are shown in Figs. 3a–3c. Figure 3d presents the details of the processing strategy designed for the 20 min of total polishing time. Samples A and B are polished following the stepwise polishing, and their *Sa* roughnesses and PSD are measured every 5 min and 10 min, respectively. Sample C is continuously polished following the one-step polishing strategy, and the *Sa* roughness and PSD are measured only once after 20 min of polishing.

Results and Discussion

Critical spatial frequency.—PSD curves and the morphologies of errors at different frequency bands before and after ECP for 45 min and 90 min are shown in Fig. 4. The ECP was performed in 1% NaOH electrolyte at an applied voltage of 15 V. The experimental results intuitively present that ECP has different optimization abilities for surface errors in different frequency bands. For example, ECP did not influence PSD below the critical spatial frequency; at the same time, the PSD was significantly decreased above the critical spatial frequency, as seen from Fig. 4. The critical spatial frequency (4×10^{-6} nm^{-1}) was defined by the intersection of PSD curves before and after ECP. In other words, ECP technology only can optimize the error with a spatial period below 250 μm but has no obvious optimization ability for the error with a spatial period above 250 μm. Since the surface texture is a complex condition resulting from a combination of roughness (nano and micro-roughness), waviness, and lay and flaw. Therefore, the surface morphology recorded by WLI can be disintegrated into waviness and roughness errors by using the filtering method. Results from the surface error before ECP (Figs. 4a1 and 4a2) and after ECP for 45 min. (Figures. 4b1 and 4b2) and 90 min. (Figures. 4c1 and 4c2) can be obtained by applying a filter equal to the critical spatial frequency. These results provide substantial evidence that the surface error optimization by ECP is mainly the optimization of high-frequency roughness errors, while low-frequency errors are rarely influenced.

Furthermore, the effects of polishing voltage and electrolyte concentration on the critical spatial frequency were explored, as shown in Fig. 5. The PSD curves in Figs. 5a–5c are obtained after ECP in 1% NaOH electrolyte at different applied voltages (U = 10, 20, and 30 V). Similarly, the PSD curves in Figs. 5d–5f are obtained after ECP at a constant voltage of U = 15 V in different NaOH electrolyte concentrations (wt% = 0.5, 1.0, 1.5). The PSD curves in Fig. 5 show that the critical spatial frequency remained nearly independent of ECP working parameters, whereas the critical period is hundreds of microns. The PSD curves calculated from the WLI data obtained from the polished samples are relatively smooth compared to the grounded substrate, possibly due to a reduction in the *Sa* roughness after ECP. Although the PSD curves of the processed substrates are smooth nearly at all the spatial frequencies,

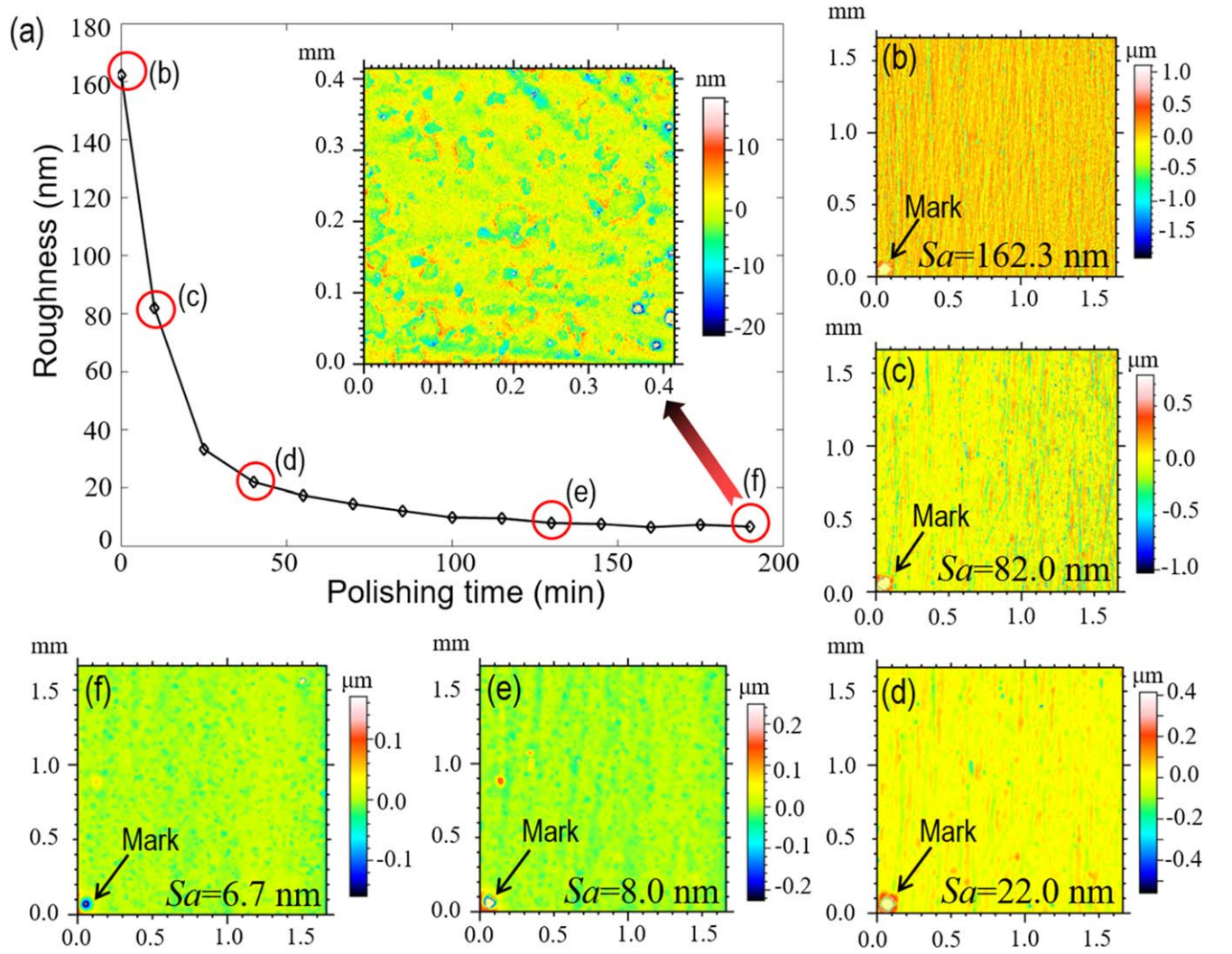

Figure 8. (a) The evolution of surface roughness of tungsten substrate measured by WLI after polishing for different durations (inset shows the microscopic features on the surface that reached the ultimate roughness); The WLI morphologies of the substrate after ECP for; (b) 0 min, (c) 10 min, (d) 40 min, (e) 130 min, (f) 190 min.

minor irregularities are observed in some regions which are not pronounced. The *Sa* roughness at different points on the processed surface does not vary significantly, and the measurement position on the surface does not significantly influence the PSD curves; hence multiple PSD measurements were not performed.

A slight increase in the low-frequency band PSD indicates an insignificant deterioration in the waviness error after ECP, as shown in Fig. 4. The deterioration may be caused by the bubbles generated during the polishing process or the formation of local micro-cells induced by the embedded abrasive particles in the lapping process.

In addition, the effects of initial surface roughness on the critical spatial frequency are also explored, as shown in Fig. 6. The ECP is performed on two samples with initial surface roughness of ∼100 nm and ∼150 nm. The electrolyte concentration is 1.0 wt%, and the applied voltage is 15 V. The PSD curves in Fig. 6 show that the critical frequency remained nearly independent of initial surface roughness since the difference in initial roughness originating from the grinding with different sandpapers is the main source of high-frequency errors.

The PSD curve slightly raised in the low-frequency range and sharply decreased in the high-frequency range after ECP. Therefore, PSD curves before and after ECP intersect and define the critical spatial frequency (f_c). Therefore, the critical spatial frequency in ECP is essentially the result of the difference in the control ability on different frequency band errors and the slight deterioration of waviness error.

Ultimate roughness of ECP.—Figure 7 presents the *Sa* roughness and PSD curves after stepwise polishing and one-step polishing. According to Fig. 7a, two rounds of 5 min stepwise polishing (total 10 min) achieved a *Sa* roughness similar to that of one-step polishing for 10 min. Similarly, two rounds of 10 min stepwise polishing (total 20 min) achieved a *Sa* roughness similar to that of one-step polishing for 20 min. So we can infer that the *Sa* roughness achieved by ECP conducted under fixed conditions is independent of stepwise and one-step polishing unless the total polishing duration is the same. Fig. 7b shows the PSD curves of the three samples. These results also endorse that the surface errors processed by the two strategies are also similar over a range of spatial frequency bands. Therefore, using the stepwise polishing strategy in the ultimate roughness experiments is feasible.

The results of ECP ultimate roughness experiments are shown in Fig. 8. The variation in *Sa* roughness as a function of polishing time is shown in Fig. 8a. Initially, the *Sa* roughness decreased rapidly with an optimization efficiency greater than 8 nm min^{-1}. $A^{-1}s^{-1}$ ECP progressed, the optimization efficiency was quickly reduced. For instance, the optimization efficiency of *Sa* roughness was reduced to less than 0.1 nm min^{-1} after ECP for 100 min. After

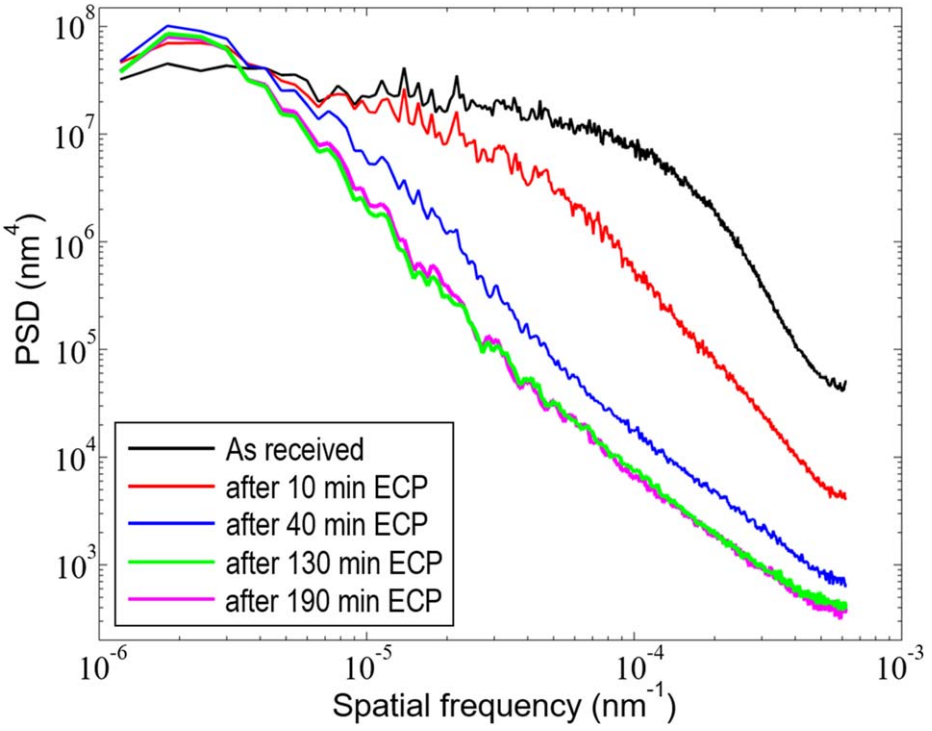

Figure 9. The PSD curves before and after ECP with different ECP durations.

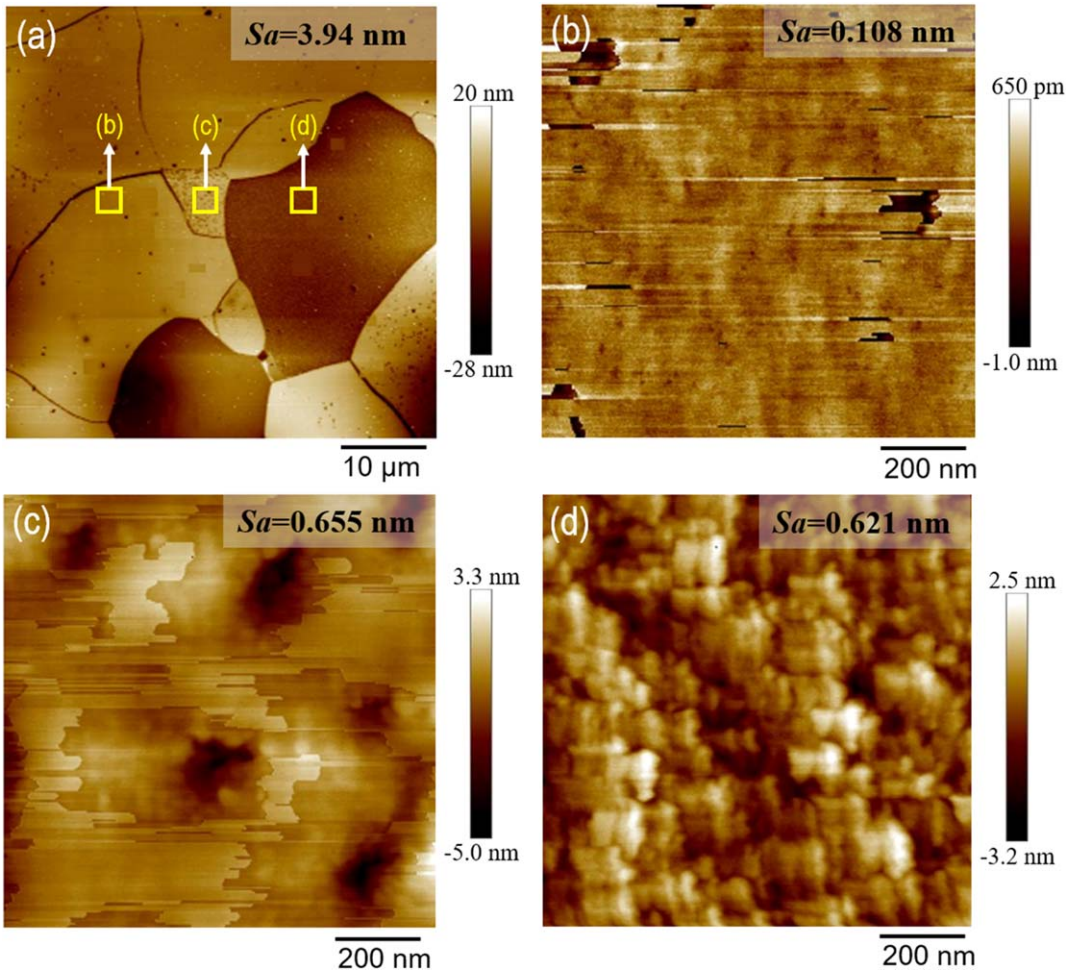

Figure 10. (a) AFM morphology of concave region, and (b)–(d) micro-morphologies of different areas on the surface that reached the ultimate roughness.

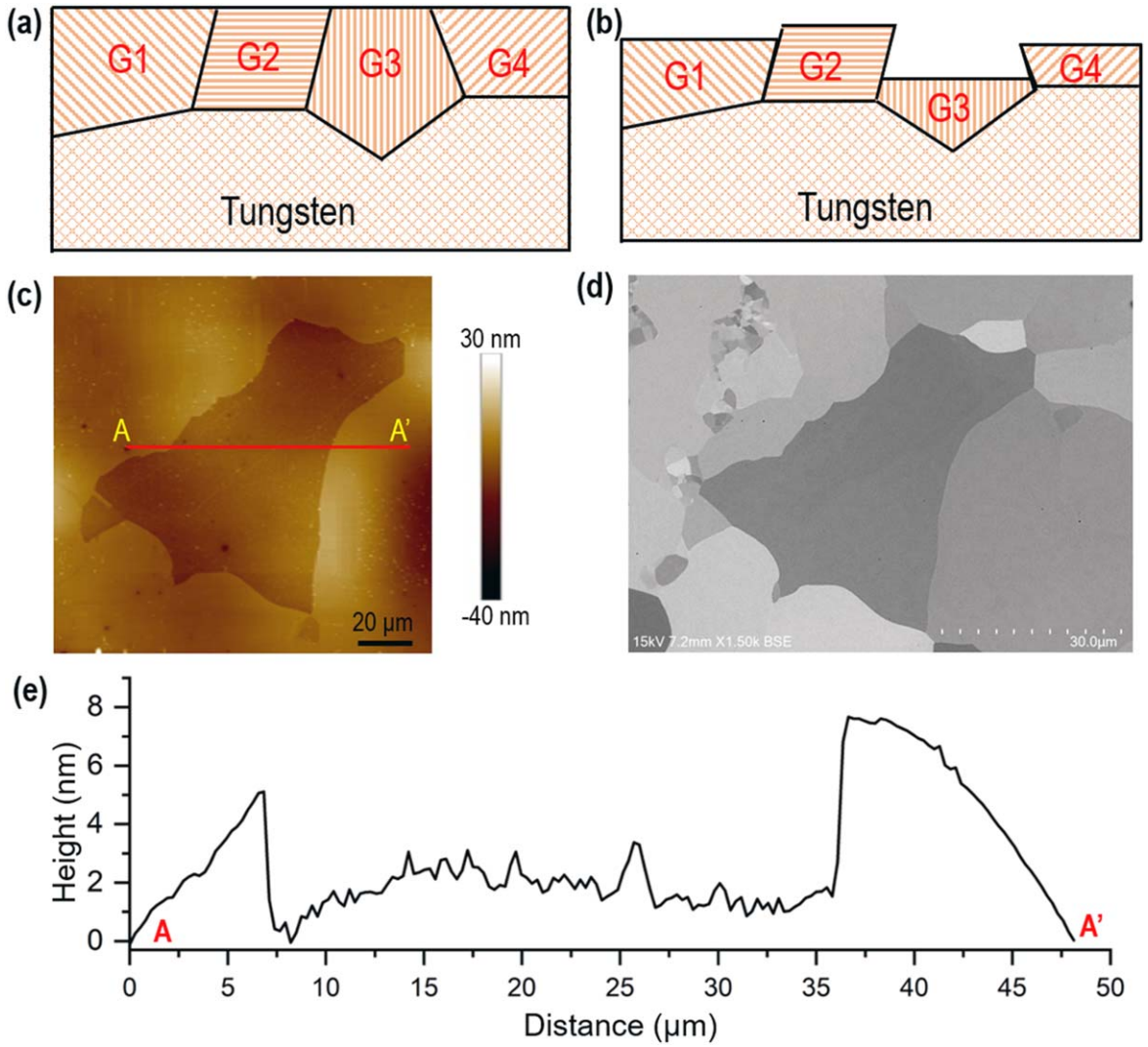

Figure 11. Schematic of the crystal corrosion during ECP (a) before polishing, (b) after polishing, surface; corrosion pit morphologies by (c) AFM, (d) SEM, and (f) line profile.

160 min of ECP, the *Sa* roughness remained practically unchanged, indicating that the ECP ultimate roughness had been reached. Figs. 8b–8f show the WLI morphologies and the *Sa* roughness after ECP for 0 min, 10 min, 40 min, 130 min, and 190 min. As ECP progressed, surface fluctuation gradually smoothed, and the grinding marks were completely removed. In order to further explore the reasons behind the ultimate roughness of ECP, the surface that reached the ultimate roughness (Fig. 8f) was further analyzed. In this case, a smaller area (410 × 410 μm^2) was measured by WLI, as shown in the inset in Fig. 8a. Many micro-concave features with a scale of tens of microns appeared on the surface, which seriously hindered the further optimization of surface roughness. In addition, the evolution of PSD curves with duration is presented in Fig. 9. Initially, the PSD curve rapidly decreased with increasing ECP duration (up to 130 min) but coincided for 130 and 190 min, indicating that the ultimate roughness had been reached, which is in good agreement with the results shown in Fig. 8. Obviously, the critical spatial frequency did not change significantly as ECP progressed.

The surface with ultimate roughness was further measured by AFM over an area of 50 × 50 μm^2, as shown in Fig. 10a. The micro-concave features are irregular, and the micro-morphologies of different regions on the surface were further measured over 1 × 1 μm^2, as shown in Figs. 10b–10d. The AFM morphologies measured from these regions show obvious differences in surface roughness and micro-morphologies. In Fig. 10a, region (b) is relatively flat, and the roughness is only 0.1 nm, whereas region (c) and region (d) are not very smooth, and the roughness is greater than 0.6 nm. In addition, the micro-morphologies of region (c) and region (d) are entirely different. According to the material removal principle of ECP and the surface micro-morphology after polishing, the micro-concave regions might be formed due to crystal corrosion. Therefore the different micro-morphologies might be caused by the different atomic configurations on different crystal planes. The irregular cracks in Fig. 10a may result in preferential corrosion at the crystal boundaries.

As shown in Figs. 11a, 11b, G1, G2, G3, and G4 represent different crystal planes. Variable corrosion rates emerge from different atomic configurations in crystal planes during polishing, generating visible corrosion pits with grain boundaries on the surface. The argument of crystal corrosion was supported by further surface characterization. The corrosion pits at the same position on the surface that reached the ultimate roughness were measured by AFM and SEM. The results are shown in Figs. 11c, 11d. The shape of micro corrosion pits measured by AFM is consistent with that measured by SEM, which strongly supports that corrosion pits are formed due to different corrosion rates. The line profile of the corrosion pit given in Fig. 11e shows that the corrosion pit is nearly 5 nm deep. Interestingly, the corrosion pit depth is of the same order of magnitude as the ultimate roughness of ECP. Therefore, the

formation of the corrosion pit will have a great influence on the ultimate roughness of ECP. In conclusion, the phenomenon of crystal corrosion is the fundamental factor inhibiting further convergence of *Sa* roughness during ECP.

Conclusions

ECP technology has many unique advantages over traditional polishing technologies because of its anode dissolving material removal approach. Enormous literature on ECP parametric optimization and the effect of working conditions on the final surface quality can be found. However, the ultimate roughness of ECP, factors inhibiting further *Sa* roughness optimization, and the range of spatial frequencies that ECP can correct are rarely addressed. This paper exclusively focuses on these issues and brings to light the concepts of critical spatial frequency and ultimate roughness of ECP. The relevant conclusions are as follows:

1. The critical spatial frequency of ECP is about hundreds of microns, and it is difficult for ECP to correct the surface error with a spatial wavelength greater than that. Since the ECP processing parameters do not influence the critical spatial frequency, the critical spatial frequency can be used as a filter to accurately determine the polishing ability of ECP.
2. Given that the other ECP conditions remain fixed, the final *Sa* roughness is independent of polishing strategies, either stepwise polishing or one-step polishing. Therefore stepwise polishing is also suitable for ECP ultimate roughness experiments.
3. The surface optimization speed rapidly decreases with reducing *Sa* roughness and becomes negligible when the ultimate roughness is reached. Crystal corrosion is the fundamental factor hindering further convergence of *Sa* roughness during ECP.

Acknowledgments

This work is financially supported by the National Natural Science Foundation of China (Grant No. 52035009, 52005243) and the research fund from the Science and Technology Innovation Committee of Shenzhen Municipality (JCYJ20200109141003910), Shenzhen, China. The authors acknowledge the assistance of SUSTech Core Research Facilities.

CRediT Authorship Contribution Statement

Ji Jianwei: Conceptualization, Investigation, Formal analysis, Visualization, Methodology, Writing-original draft, Writing-review&editing. **Khan Muhammad Ajmal**: Investigation, Validation, Writing-review&editing. **Zhan Zejin**: Visualization. **Yi Rong**: Writing-review&editing. **Deng Hui**: Supervision, Resources.

Declaration of Competing Interest

The authors declare that they have no known competing financial interests or personal relationships that could have appeared to influence the work reported in this paper.

ORCID

Deng Hui https://orcid.org/0000-0002-7116-7188

References

1. G. M. Song, Y. J. Wang, and Y. Zhou, *Int. J. Refract. Met. H.*, **21**, 1 (2003).
2. Y. Yamada, M. Kawakubo, K. Kadomura, T. Sugaya, O. Hirai, and K. Tsugane, *J. Electrochem. Soc.*, **157**, H617 (2010).
3. N. Suzuki, M. Haritani, J. Yang, R. Hino, and E. Shamoto, *CIRP Ann. Manuf. Technol.*, **56**, 127 (2007).
4. J. W. Dams, V. R. Barabash, A. Makhankov, L. Plochl, and S. K. Slattery, *J. Nucl. Mater.*, **258–263**, 308 (1998).
5. H. G. Prengel, A. T. Santhanamb, R. M. Penich, P. C. Jindal, and K. H. Wendt, *Surf. and Coat. Tech.*, **94–95**, 597 (1997).
6. E. Paul, *J. Electrochem. Soc.*, **148**, 359 (2001).
7. Y. Zhang, Z. Zhou, Y. Lv, J. Wang, L. Shao, and A. Iqbal, *Int. J. Adv. Manuf. Technol.*, **69**, 329 (2013).
8. S. N. Joshi and S. S. Pande, *J. Manuf. Process.*, **12**, 45 (2010).
9. S. Glarum and J. Marshall, *J. Electrochem. Soc.*, **132**, 2872 (1985).
10. W. Han and F. Z. Fang, *Int. J. Mach. Tools Manuf*, **139**, 1 (2019).
11. K. M. Ajmal, R. Yi, Z. J. Zhan, J. W. Ji, and H. Deng, *Precis. Eng.*, **71**, 119 (2021).
12. X. Y. Zhou, F. Wang, X. Q. Zhang, and H. Deng, *J. Mater. Process. Tech.*, **292**, 117055 (2021).
13. A. G. Gallegos, F. Mill, and A. R. Mount, *J. Manuf. Process.*, **23**, 83 (2016).
14. H. Deng, R. Huang, K. Liu, and X. Q. Zhang, *Electrochem. Commun.*, **82**, 80 (2017).
15. F. Wang, X. Zhang, and H. Deng, *Appl. Surf. Sci.*, **475**, 587 (2019).
16. W. Han and F. Z. Fang, *Adv. Manuf.*, **8**, 265 (2020).
17. Y. G. Li, H. Takino, and F. Frost, *Opt. Express*, **25**, 7828 (2017).
18. X. Q. Nie, S. Y. Li, H. Hu, and Q. Li, *Appl. Optics*, **53**, 6332 (2014).
19. C. S. Murthy, D. Wang, S. P. Beaudoin, T. Bibby, K. Holland, and T. S. Cale, *Thin Solid Films*, **308**, 533 (1997).
20. P. A. Jacquet, *Nature*, **135**, 1076 (1935).
21. T. P. Hoar and T. W. Farthing, *Nature*, **169**, 324 (1952).
22. J. W. Ji, W. Fan, W. Gao, C. Wang, Y. F. Zhang, M. Xu, and F. Ji, *Appl. Optics*, **58**, 5388 (2019).
23. J. M. Elson and J. M. Bennett, *Appl. Optics*, **34**, 201 (1995).
24. J. H. Hoyo, H. Choi, J. H. Burge, G. H. Kim, and D. W. Kim, *Appl. Optics*, **56**, 5258 (2017).
25. N. I. Chkhalo, S. A. Churin, A. E. Pestov, N. N. Salashchenko, Y. A. Vainer, and M. V. Zorina, *Opt. Express*, **22**, 20094 (2014).
26. J. Kim, J. K. Park, H. K. Kim, A. R. Unnithan, C. S. Kim, and C. H. Park, *J. Nanosci. Nanotechnol.*, **17**, 2333 (2017).
27. P. Lochynski, A. Sikora, and B. Szczygiel, *Surf. Eng.*, **33**, 395 (2017).
28. S. G. Choi, S. H. Kim, W. K. Choi, and E. S. Lee, *Int. J. Adv. Manuf. Tech.*, **82**, 1933 (2016).